FULL PAPER

ScFv-Decorated PEG-PLA-Based Nanoparticles for Enhanced siRNA Delivery to Her2$^+$ Breast Cancer

Shuang Dou, Xian-Zhu Yang, Meng-Hua Xiong, Chun-Yang Sun, Yan-Dan Yao, Yan-Hua Zhu, and Jun Wang**

Patients with Her2-overexpressing (Her2$^+$) breast cancers generally have a poorer prognosis due to the high aggressiveness and chemoresistance of the disease. Small interfering RNA (siRNA) targeting the gene encoding polo-like kinase 1 (Plk1; si*Plk1*) has emerged as an efficient therapeutic agent for Her2$^+$ breast cancers. Poly(ethylene glycol)-*block*-poly(D,L-lactide) (PEG-PLA)-based nanoparticles for siRNA delivery were previously developed and optimized. In this study, for targeted delivery of si*Plk1* to Her2$^+$ breast cancer, anti-Her2 single-chain variable fragment antibody ($ScFv_{Her2}$)-decorated PEG-PLA-based nanoparticles with si *Plk1* encapsulation ($ScFv_{Her2}$-NP_{si} *Plk1*) are developed. With the rationally designed conjugation site, $ScFv_{Her2}$-NP_{siRNA} can specifically bind to the Her2 antigen overexpressed on the surface of Her2$^+$ breast cancer cells. Therefore, $ScFv_{Her2}$-NP_{si} *Plk1* exhibits improved cellular uptake, promoted Plk1 silencing efficiency, and induced enhanced tumor cell apoptosis in Her2$^+$ breast cancer cells, when compared with nontargeted NP_{si} *Plk1*. More importantly, $ScFv_{Her2}$-NP_{siRNA} markedly enhances the accumulation of siRNA in Her2$^+$ breast tumor tissue, and remarkably improves the efficacy of tumor suppression. Dose-dependent anti-tumor efficacy further demonstrates that $ScFv_{Her2}$-decorated PEG-PLA-based nanoparticles with si*Plk1* encapsulation can significantly enhance the inhibition of Her2$^+$ breast tumor growth and reduce the dose of injected siRNA. These results suggest that $ScFv_{Her2}$-decorated PEG-PLA-based nanoparticles show great potential for targeted RNA interference therapy of Her2$^+$ breast tumor.

1. Introduction

Breast cancer has emerged as the most commonly diagnosed type of cancer among women in the world.[1] About 20% to 35% of invasive breast carcinomas overexpress human epidermal growth factor receptor 2 (Her2/neu),[2] which has been considered as an important molecular marker for clinical practice.[3] Patients harboring Her2/neu-positive breast cancers generally have a poorer prognosis because of the high aggressiveness and chemoresistance of the disease.[4] Trastuzumab (anti-Her2 monoclonal antibody) has become one of the most effective treatments for Her2-overexpressing (Her2$^+$) breast cancers;[5] however, about 15% of trastuzumab-treated patients progress to develop metastatic disease, and nearly 60% of patients with Her2$^+$ metastatic breast cancers do not respond to the treatment.[6] Therefore, additional efficient therapies are needed.

The gene-encoding polo-like kinase 1 (Plk1), which is a highly conserved serine-threonine kinase that promotes cell division, shows elevated activity in many cancers and correlates with aggressive behavior,[7] including Her2$^+$ breast cancer.[8] As reported, downregulation of Plk1 gene expression induces cell cycle arrest, apoptosis, and "mitotic catastrophe" in cancer cells,[9] rendering Plk1 an attractive therapeutic target.[10] A few of the small molecule inhibitors of Plk1 protein are now under clinical trials at different stages.[11] Small interfering RNA (siRNA) is a potent therapeutic agent for numerous diseases because of its ability to silence specific genes rapidly and efficiently,[12] and si*Plk1* has been demonstrated to be an efficient alternative.[9] In our previous studies, we have also demonstrated that nanoparticles carrying si*Plk1* can efficiently suppress breast cancer growth.[13] Moreover, it has been demonstrated that hybrid nanoparticles of PEG–PLA with a cationic lipid can encapsulate siRNA at a very high efficiency, and systemic delivery of siRNA with such nanoparticles can inhibit cancer growth in relevant murine models.[14] The approach is versatile and completely different from the existing formulation of polyplexes or lipoplexes, and importantly, as it is based on biocompatible components, it should facilitate technology transfer and clinical translation when it is considered that block copolymer of poly(ethylene glycol) and poly(D,L-lactide-*co*-glycolide) has been formulated with paclitaxel into a nanoparticle formulation (Genexol-PM) for breast cancer treatment.[15] However, after passive accumulation at the tumors tissue via the enhanced permeability and retention (EPR) effect, this delivery system can not specifically deliver si*Plk1* to Her2$^+$ breast cancer.

Dr. S. Dou, Dr. X.-Z. Yang, Dr. M.-H. Xiong, C.-Y. Sun, Prof. Y.-D. Yao, Y. H. Zhu, Prof. J. Wang
Hefei National Laboratory for Physical Sciences at Microscale
and School of Life Sciences
University of Science and Technology of China
Hefei, Anhui 230027, P. R. China
E-mail: jwang699@ustc.edu.cn; yangxz@hfut.edu.cn
Prof. Y.-D. Yao
Department of Breast Surgery
No.2 Affiliated Hospital of Sun Yat-Sen University
Guangzhou 510120, P. R. China
Prof. J. Wang
High Magnetic Field Laboratory of CAS
University of Science and Technology of China
Hefei, Anhui 230026, P. R. China

DOI: 10.1002/adhm.201400037

Previous studies showed that the attachment of targeting ligand onto the surface of the delivery systems can bind specifically to the target cell,[16] which can enhance the internalization of nanoparticles via receptor-mediated endocytosis and thus has the potential to significantly improve therapeutic efficacy and reduce the injection dose. Up to now, a variety of tumor targeting ligands, such as antibodies,[17] peptides,[18] small molecules,[19] and aptamer,[20] have been developed to enhance the uptake of nanoparticles into tumor cells. Among them, the monoclonal antibodies have been widely used to decorate drug delivery nanoparticles due to the high affinity and specifically binding to the target cells. However, the high molecular weight of the full-length antibody, immunogenicity, and high cost limit the wide use of this antibody as a ligand for tumor-targeted nanoparticles. To overcome these problems, single-chain variable fragment (ScFv) antibody has been firstly cloned by Bird et al. and Huston et al. in 1988,[21] and the ScFv-decorated cationic liposome as plasmid DNA delivery system (SGT-53) has been developed by SynerGene Therapeutics Inc. By comparison with the intact antibody as a targeting ligand, the ScFv possesses many advantages, including 1) low molecular weight, 2) small size, 3) less immunogenicity. Moreover, the ScFv conjugated to the nanoparticle surface demonstrates multivalent binding to receptors due to the multiple copies of ScFv on the nanoparticle surface,[22] which can efficiently overcome the disadvantage that its binding affinities are lower than that of the intact antibody. Thus the ScFv are particularly suitable for engineering-targeted nanoparticles. For Her2$^+$ breast cancer, the accessibility of the extracellular domain of Her2 makes it an ideal marker for the receptor-mediated drug delivery systems. Recently, we have reported that a fusion protein can even specifically deliver si*Plk1* to Her2$^+$ breast cancer to suppress Her2$^+$ breast cancer growth and metastasis.[23] Therefore, the anti-Her2 ScFv ($ScFv_{Her2}$) emerged as a promising ligand to target the Her2$^+$ breast cancer.

In this study, in order to more specifically deliver si*Plk1* to Her2$^+$ breast cancer, we developed $ScFv_{Her2}$-decorated PEG–PLA nanoparticles ($ScFv_{Her2}$-NP) with si*Plk1* encapsulation by conjugation of the C-terminal cysteine containing $ScFv_{Her2}$ on its surface (**Figure 1**). To reveal the enhanced siRNA delivery efficiency by $ScFv_{Her2}$ decoration, cellular uptake, gene-silencing efficacy, and cell apoptosis were observed in Her2$^+$ and Her2$^-$ breast cancer cells. Furthermore, we evaluated siRNA accumulation and the inhibition of tumor growth in Her2$^+$ and Her2$^-$ breast tumor xenografts. Finally, dose-dependent anti-cancer efficiency was investigated to demonstrate the advantage of the $ScFv_{Her2}$-NP_{siRNA} formulation in the treatment of Her2$^+$ breast cancers.

2. Results and Discussion

2.1. Expression and Purification of $ScFv_{Her2}$ Containing C-Terminal Cysteine

ScFv was used to decorate the siRNA-encapsulated nanoparticles because it possesses a much lower molecular weight but exhibits greater biophysical stability and lessened immunogenicity compared with the full-length antibody.[24] Retaining high affinity of $ScFv_{Her2}$ is important to specifically deliver

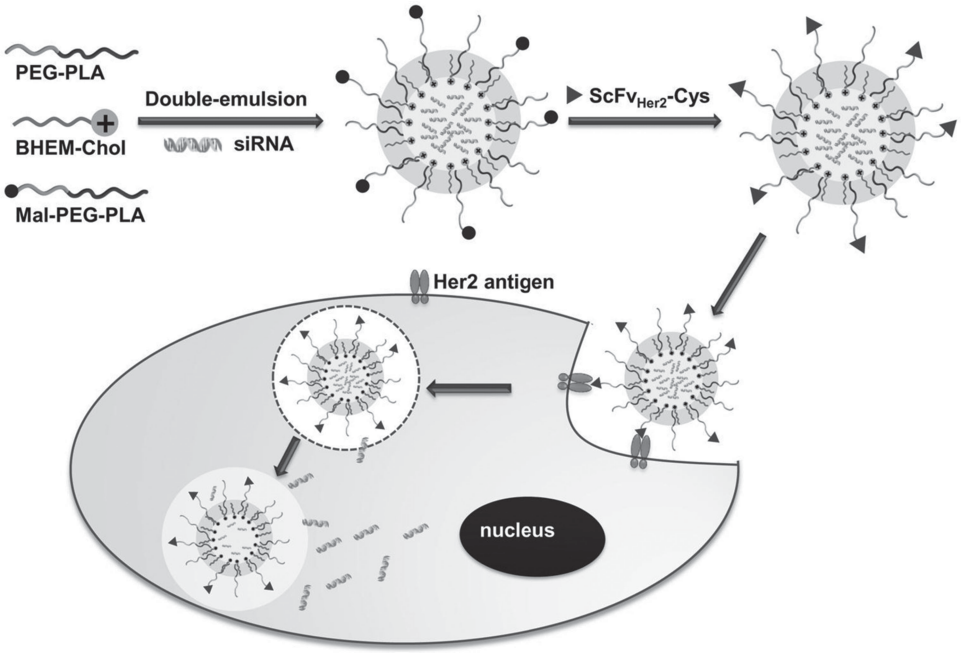

Figure 1. Schematic illustration of the preparation of $ScFv_{Her2}$-decorated PEG-PLA nanoparticles with siRNA encapsulation ($ScFv_{Her2}$-NP_{siRNA}), and the potential route for intracellular internalization of $ScFv_{Her2}$-NP_{siRNA} by Her2$^+$ breast cancer cells via Her2 antigen-mediated endocytosis. PEG–PLA: methoxy-terminated poly(ethylene glycol)-block-poly(D,L-lactide) copolymer; BHEM-Chol: cationic lipid *N*,*N*-bis(2-hydroxyethyl)-*N*-methyl-*N*-(2-cholesteryloxycarbonyl aminoethyl) ammonium bromide; Mal-PEG-PLA: maleimide-terminated poly(ethylene glycol)-block-poly(D,L-lactide); $ScFv_{Her2}$-Cys: anti-Her2 ScFv with Cys at its C-terminus.

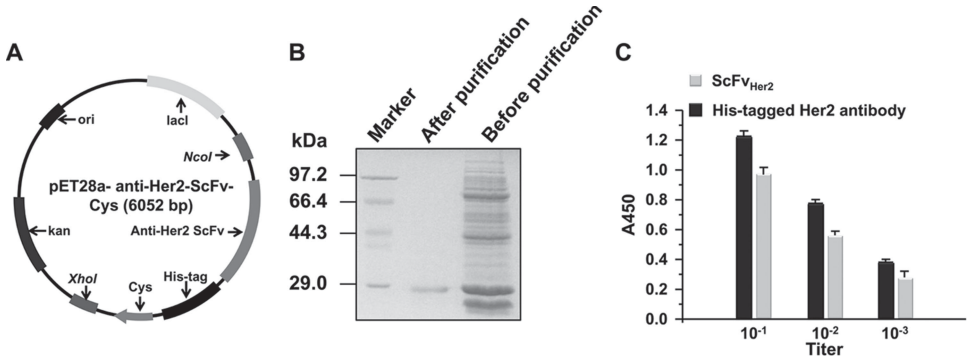

Figure 2. Expression, purification, and identification of the ScFv$_{Her2}$-Cys fusion protein. A) Map of the plasmid pET28a-Her2 ScFv-Cys. B) Detection of ScFv$_{Her2}$-Cys purified from the lysates of bacterial cells using imidazole by SDS-PAGE with Coomassie Blue staining. C) Determination of immunoactivity of ScFv$_{Her2}$-Cys using ELISA.

si*Plk1* to Her2$^+$ breast cancer using ScFv$_{Her2}$-NP$_{siRNA}$. To avoid decreasing the affinity of ScFv$_{Her2}$, the conjugation of ScFv$_{Her2}$ to the surface of siRNA-encapsulated nanoparticles should carry out under mild reaction conditions, and the conjugation site should far away from the antibody binding site.[25] To overcome this challenge, we used the expression vector pET28a cloned with an expression cassette for an anti-Her2 ScFv with a six-histidine tag linked to its C-terminus and followed by Cys (**Figure 2**A). The His$_6$ tag at the C terminus facilitated purification of recombinant protein ScFv$_{Her2}$ with a C-terminal cysteine (ScFv$_{Her2}$-Cys) by chromatography on Ni-NTA-agarose. The collected protein was analyzed by 12% sodium dodecyl sulfate polyacrylamide gel electrophoresis (SDS-PAGE) and stained by Coomassie Blue. As shown in Figure 2B, Coomassie Blue staining revealed a ≈28-kDa band, and optical density analyses of the bands indicated a >90% purity of ScFv$_{Her2}$-Cys.

The obtained ScFv$_{Her2}$-Cys, containing a thiol group, can be chemically conjugated onto the surface of the siRNA-loaded NP (NP$_{siRNA}$) via a facile thiol-maleimide coupling reaction under mild conditions, which is widely used for ligand–polymer conjugates.[26] Moreover, the ScFv$_{Her2}$-Cys construct contains heavy chain (VH) and light chain (VL) variable regions linked by a flexible peptide [-(Gly)$_4$-Ser-]$_3$ motif, and the ScFv$_{Her2}$-Cys has a C-terminal Cys peptide that directs conjugation away from the antibody's binding site. We also determined the immunoactivity of ScFv$_{Her2}$-Cys binding to Her2 antigen using ELISA. ScFv$_{Her2}$-Cys proteins and human anti-Her2 antibody were each incubated with cell lysates from Her2$^+$ BT474 cancer cells. Our results showed that ScFv$_{Her2}$-Cys exhibited nearly the same antigen-binding capability as Her2 monoclonal antibody (Figure 2C).

2.2. Preparation and Characterization of ScFv$_{Her2}$-NP$_{siRNA}$

ScFv$_{Her2}$-NP$_{siRNA}$ was prepared by two-step methods consisting of double emulsion and bioconjugation. With the assistance of the cationic lipid BHEM-Chol, about 95.9% of total siRNA was encapsulated into the nanoparticles. Then, ScFv$_{Her2}$-Cys was chemically conjugated onto the surface of siRNA-loaded nanoparticles (NP$_{siRNA}$) through a covalent thiol-maleimide linkage at equal molar ratio in PB buffer (pH 6.8) for 12 h. The supernatant of the reaction solution was collected and analyzed by SDS-PAGE followed by Coomassie Blue staining. As shown in **Figure 3**A, a 28-kDa band corresponding to the size of ScFv$_{Her2}$-Cys was clearly displayed for the mixture of ScFv$_{Her2}$-Cys and Mal-NP$_{siRNA}$ without incubation. In contrast, the band was almost disappeared after 12 h incubation. The residual amounts of thiol groups were determined with Ellmann's reagent, which showed that 80.7% of ScFv$_{Her2}$-Cys was conjugated

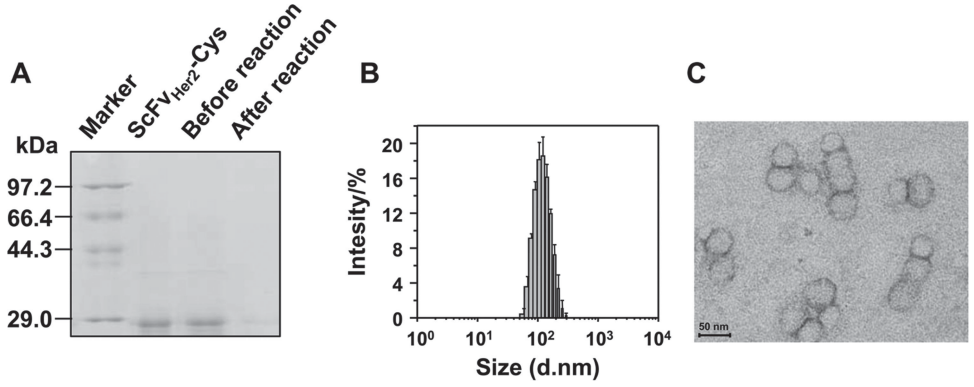

Figure 3. A) Assessment of the conjugation of ScFv$_{Her2}$ to the surface of Mal-NP$_{siRNA}$ through a covalent thiol-maleimide linkage by SDS-PAGE with Coomassie Blue staining. B) Intensity distribution of particle size of ScFv$_{Her2}$-NP$_{siRNA}$. C) Transmission electron microscopy image of ScFv$_{Her2}$-NP$_{siRNA}$.

to the surface of siRNA-loaded Mal-NP_{siRNA}. The residual maleimide groups of the $ScFv_{Her2}$-NP_{siRNA} were quenched by reaction with cysteine before the subsequent studies.

The average size of $ScFv_{Her2}$-NP_{siRNA} was about 120 nm (Figure 3B), which were similar to those of nontargeted NP_{siRNA} (data not shown). For structural characterization, $ScFv_{Her2}$-NP_{siRNA} was imaged by transmission electronic microscopy (TEM), showing a compact and spherical morphology (Figure 3C). Furthermore, $ScFv_{Her2}$-NP_{siRNA} and NP_{siRNA} showed similar drug release rates, exhibiting about 22% siRNA release from both nanoparticles after 48 h incubation in phosphate buffered saline (PBS) (Figure S1, Supporting Information). These data demonstrated that $ScFv_{Her2}$-NP_{siRNA} and NP_{siRNA} possessed similar properties and comparable siRNA release rates, which offered substantial advantage for the evaluation of their internalization, gene-silencing efficiency, inhibition of cell proliferation, induction of cell apoptosis, and accumulation in solid tumors as well as the associated tumor growth suppression, to assess the ability of $ScFv_{Her2}$ decoration to specifically deliver si*Plk1* to $Her2^+$ breast cancer.

2.3. $ScFv_{Her2}$-NP_{siRNA} Enhanced the Uptake of siRNA in $Her2^+$ Breast Cancer Cells

Previous studies showed that a targeting ligand can bind specifically to the target cell and improve the internalization of nanoparticles via receptor-mediated endocytosis.[27] The Her2 antigen is a member of the HER family of transmembrane receptor tyrosine kinases,[28] and siRNA-encapsulated nanoparticles with $ScFv_{Her2}$ decoration were expected to specifically bind to $Her2^+$ breast tumor cells through overexpressed antigens on the surface, entering the cell via Her2 receptor-mediated endocytosis. To demonstrate this, the internalization of $ScFv_{Her2}$-$NP_{FAM\text{-}siRNA}$ or nontargeted $NP_{FAM\text{-}siRNA}$ into $Her2^+$ BT474 and $Her2^-$ MDA-MB-231 cells was examined by flow cytometry. After incubation with fluorescent FAM-siRNA-encapsulated nanoparticles at 37 °C for 1 h, intracellular fluorescence was analyzed by flow cytometry. As shown in **Figure 4**, $Her2^+$ BT474 cells incubated with $ScFv_{Her2}$-$NP_{FAM\text{-}siRNA}$ showed much stronger green fluorescence compared with those incubated with nontargeted $NP_{FAM\text{-}siRNA}$. On the contrary, no significant difference was observed in the $Her2^-$ MDA-MB-231 cells after incubation with either $ScFv_{Her2}$-$NP_{FAM\text{-}siRNA}$ or nontargeted $NP_{FAM\text{-}siRNA}$. It is noteworthy that the incubation of free FAM-siRNA alone exhibited minimal cell fluorescence. Furthermore, addition of free $ScFv_{Her2}$ significantly hindered the $Her2^+$ BT474 cellular uptake of $ScFv_{Her2}$-$NP_{FAM\text{-}siRNA}$ (Figure S2, Supporting Information). These results demonstrated that $ScFv_{Her2}$ decoration enhanced the delivery of siRNA to $Her2^+$ breast cancer.

The enhanced cellular uptake was further corroborated by observations made by confocal laser scanning microscopy. $Her2^+$ BT474 cells and $Her2^-$ MDA-MB-231 cells cultured with $ScFv_{Her2}$-$NP_{Cy5\text{-}siRNA}$ or nontargeted $NP_{Cy5\text{-}siRNA}$ for 1 h were stained with FITC-labeled Her2 antibody and 6-diamidino-2-phenylindole (DAPI). As shown in Figure S3 (Supporting Information), $Her2^+$ BT474 cells cultured with $ScFv_{Her2}$-$NP_{Cy5\text{-}siRNA}$ showed much stronger cellular red fluorescence signals than cells treated with nontargeted $NP_{Cy5\text{-}siRNA}$. In contrast, no significant difference was observed in the $Her2^-$ MDA-MB-231 cells. These results demonstrated that $ScFv_{Her2}$ decoration could more specifically bind to $Her2^+$ breast tumor cells, and subsequently enhanced siRNA delivery into $Her2^+$ breast tumor cells.

2.4. $ScFv_{Her2}$-$NP_{si\mathit{Plk1}}$ Enhanced Gene-Silencing Efficiency in $Her2^+$ Breast Cancer Cells

We then investigated whether $ScFv_{Her2}$ decoration could enhance gene-silencing efficiency in $Her2^+$ breast cancer cells. The efficiency of the si*Plk1* delivery of $ScFv_{Her2}$-NP was evaluated in $Her2^+$ BT474 and $Her2^-$ MDA-MB-231 cells. Different formulations were incubated with the cancer cells. Plk1 gene expression at both the mRNA and protein levels was determined by reverse transcription-polymerase chain reaction (RT-PCR) and Western blot analysis. As shown in **Figure 5**, the negative controls (free si*Plk1*, $ScFv_{Her2}$-$NP_{si\mathit{N.C.}}$, blank $ScFv_{Her2}$-NP, and nontargeted NP without siRNA encapsulation) did not exhibit notable efficiency in terms of silencing Plk1 gene expression. Both targeted nanoparticles and nontargeted nanoparticles carrying si*Plk1* led to efficient knockdown of Plk1 gene expression, and increasing the dose of si*Plk1* markedly improved the level of knockdown. However, in $Her2^+$ BT474 cells, $ScFv_{Her2}$-

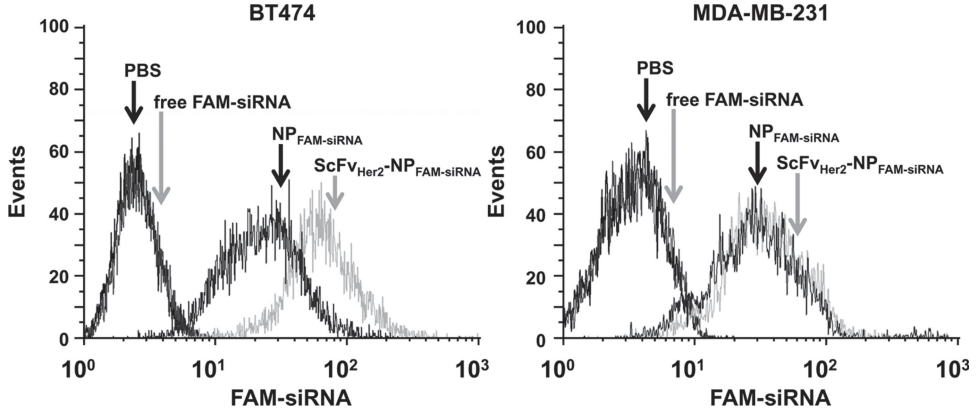

Figure 4. Flow cytometric analyses of $Her2^+$ BT474 cells and $Her2^-$ MDA-MB-231 cells after 1 h incubation with $ScFv_{Her2}$-$NP_{FAM\text{-}siRNA}$ or nontargeted $NP_{FAM\text{-}siRNA}$. The dose of FAM-siRNA was 50×10^{-9} M in the cell culture, and free FAM-siRNA was used as the negative control.

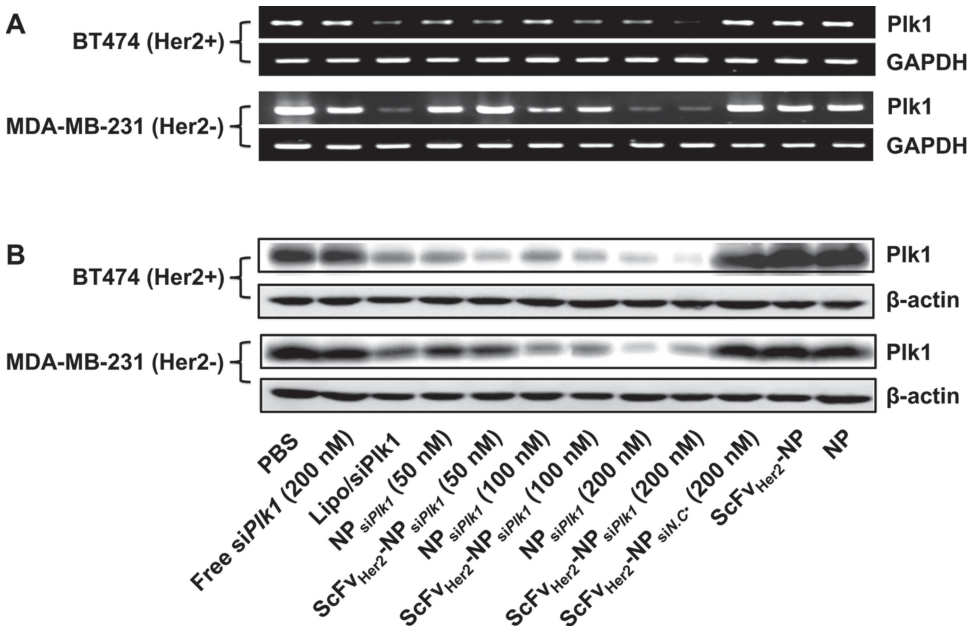

Figure 5. A) Expression levels of Plk1 mRNA in Her2$^+$ BT474 cells and Her2$^-$ MDA-MB-231 cells after transfection with $ScFv_{Her2}$-$NP_{si\mathit{Plk1}}$, nontargeted $NP_{si\mathit{Plk1}}$, and other controls. B) Plk1 protein expression in Her2$^+$ BT474 cells and Her2$^-$ MDA-MB-231 cells after transfection with $ScFv_{Her2}$-$NP_{si\mathit{Plk1}}$, nontargeted $NP_{si\mathit{Plk1}}$, and other controls. $ScFv_{Her2}$-NP and NP represent $ScFv_{Her2}$-conjugated or non-conjugated PEG-PLA-based nanoparticles without siRNA encapsulation, respectively.

$NP_{si\mathit{Plk1}}$ significantly improved the silencing efficiency of Plk1 expression at both the gene and protein levels compared with nontargeted $NP_{si\mathit{Plk1}}$, while treatment with $ScFv_{Her2}$-$NP_{si\mathit{Plk1}}$ or nontargeted $NP_{si\mathit{Plk1}}$ did not exhibit a significant difference in Her2$^-$ MDA-MB-231 cells, suggesting that $ScFv_{Her2}$-decorated nanoparticles were much more efficient in downregulating gene expression than the nontargeted nanoparticles in Her2$^+$ cells. These data were consistent with the improved uptake of siRNA via $ScFv_{Her2}$ decoration (Figure 4), and demonstrated that siRNA-encapsulated nanoparticles with $ScFv_{Her2}$ decoration could significantly improve targeted gene-silencing efficiency due to the enhanced internalization via receptor-mediated endocytosis in Her2$^+$ cells.

2.5. $ScFv_{Her2}$-$NP_{si\mathit{Plk1}}$ Enhanced Cell Proliferation Inhibition and Promoted Cell Apoptosis

Plk1 is a key regulator of the mitotic progression of mammalian cells,[29] and the activity of Plk1 is elevated in cancer cells, which contributes to the oncogenic transformation.[30] The inhibition of Plk1 can slow cell proliferation and induce cell apoptosis.[9a,31] The enhancement of Plk1 gene-silencing efficiency by $ScFv_{Her2}$-NP_{siPlk1} in Her2$^+$ cells may lead to improved inhibition of cell proliferation and induction of cell apoptosis.

To investigate whether treatment with $ScFv_{Her2}$-$NP_{si\mathit{Plk1}}$ can more efficiently inhibit Her2$^+$ cell proliferation versus $NP_{si\mathit{Plk1}}$, we incubated Her2$^+$ BT474 and Her2$^-$ MDA-MB-231 cells with the different formulations for 72 h, and cell proliferation were detected by 3-(4,5-dimethylthiazol-2-yl)-2,5-diphenyltetrazolium bromide (MTT) viability assay. As demonstrated in **Figure 6**, $ScFv_{Her2}$-$NP_{si\mathit{Plk1}}$ and $NP_{si\mathit{Plk1}}$ both inhibited the growth of Her2$^+$ BT474 cells and Her2$^-$ MDA-MB-231 cells in a dose-dependent manner. However, $ScFv_{Her2}$-$NP_{si\mathit{Plk1}}$ was much more efficient in inhibiting cell growth than the nontargeted $NP_{si\mathit{Plk1}}$ in Her2$^+$ BT474 cells (Figure 6A), especially at the si*Plk1* dose of 200×10^{-9} M (30.9% and 51.6%, respectively, $p < 0.05$). In contrast, $ScFv_{Her2}$-$NP_{si\mathit{Plk1}}$ and nontargeted $NP_{si\mathit{Plk1}}$ exhibited similar inhibition of the growth of Her2$^-$ MDA-MB-231cells (Figure 6B). It is worth noting that no significant inhibitory effect in Her2$^+$ BT474 and Her2$^-$ MDA-MB-231 cells was observed upon treatment with free si*Plk1*, nanoparticles alone ($ScFv_{Her2}$-NP and NP), or nanoparticles carrying the negative control siRNA ($ScFv_{Her2}$-$NP_{si\mathit{N.C.}}$).

To further evaluate whether treatment with $ScFv_{Her2}$-$NP_{si\mathit{Plk1}}$ can result in an elevated induction of cell apoptosis in Her2$^+$ breast cancer cells, Her2$^+$ BT474 and Her2$^-$ MDA-MB-231 cells were incubated with the above-mentioned formulations for 72 h, then the cancer cells were stained with Annexin V-FITC and propidium iodide to determine the level of cell apoptosis (**Figure 7** and Figure S4, Supporting Information). In both cell lines, empty nanoparticles, $ScFv_{Her2}$-$NP_{si\mathit{N.C.}}$, and free si*Plk1* with the same dose of siRNA did not induce remarkable cell apoptosis, while the delivery of si*Plk1* with $ScFv_{Her2}$-$NP_{si\mathit{Plk1}}$ or nontargeted $NP_{si\mathit{Plk1}}$ induced dose-dependent cell apoptosis. Compared with nontargeted NP, the enhanced cell apoptosis was only observed in Her2$^+$ BT474 cells by treating with $ScFv_{Her2}$-$NP_{si\mathit{Plk1}}$. $ScFv_{Her2}$-$NP_{si\mathit{Plk1}}$ led to 16.08% and 36.61% cell apoptosis at 100×10^{-9} and 200×10^{-9} M, respectively, while only 13.10% and 24.27% cell apoptosis was observed when the cells were treated with $NP_{si\mathit{Plk1}}$ at 100×10^{-9} and 200×10^{-9} M, respectively. However, this phenomenon was not observed in Her2$^-$ MDA-MB-231 cells; $ScFv_{Her2}$-$NP_{si\mathit{Plk1}}$ and nontargeted $NP_{si\mathit{Plk1}}$ exhibited a similar effect on apoptosis at both si*Plk1*

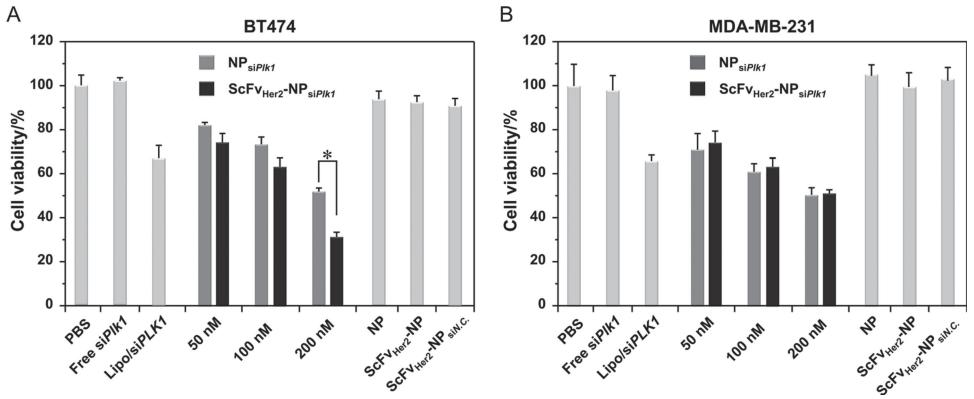

Figure 6. A,B) Cell viability of Her2$^+$ BT474 (A) and Her2$^-$ MDA-MB-231 cells (B) after transfection with ScFv$_{Her2}$-NP$_{si\textit{Plk1}}$, nontargeted NP$_{si\textit{Plk1}}$, or other controls. Lipo/si*Plk1* represents the complexes of Lipofectamine 2000 with si*Plk1* (50×10^{-9} M). Free si*Plk1* represents cells incubated with si*Plk1* at a dose of 200×10^{-9} M. NP and ScFv$_{Her2}$-NP represent cells treated with nontargeted nanoparticles and ScFv$_{Her2}$-conjugated nanoparticles without siRNA encapsulation, respectively (0.36 mg mL^{-1} of polymer). ScFv$_{Her2}$-NP$_{si\textit{N.C.}}$ represents cells transfected with ScFv$_{Her2}$-NP encapsulating si*N.C.* at a siRNA dose of 200×10^{-9} M. * $p < 0.05$ when compared with NP$_{si\textit{Plk1}}$ ($n = 3$).

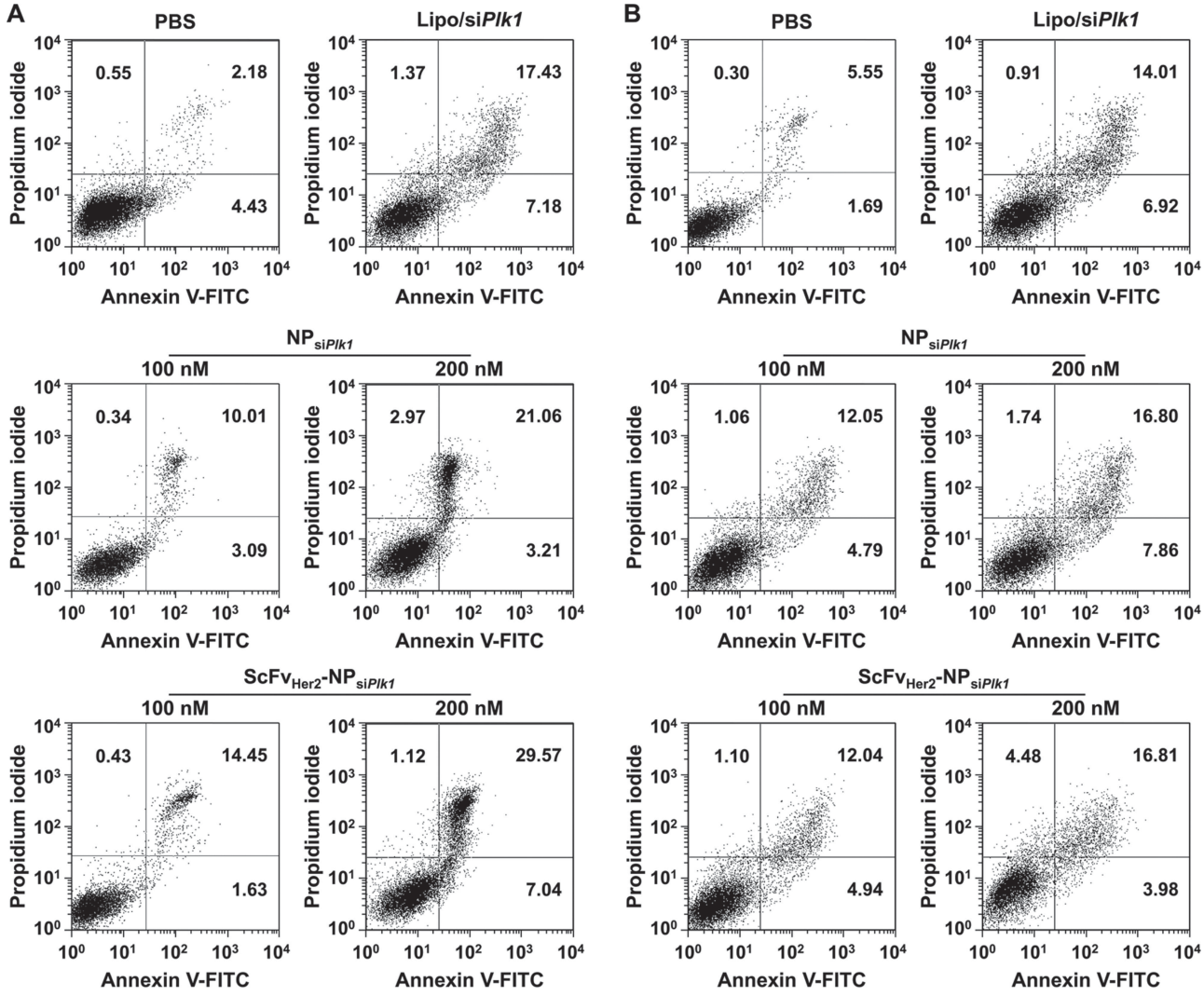

Figure 7. A,B) Induction of apoptosis of Her2$^+$ BT474 cells (A) and Her2$^-$ MDA-MB-231 (B) cells following transfection with different formulations. Early apoptotic cells are shown in the lower right quadrant and late apoptotic cells are shown in the upper right quadrant. Lipo/si*Plk1* represents the complexes of Lipofectamine 2000 with si*Plk1* (50×10^{-9} M). Cell apoptosis after treatment with other controls is given in the Supporting Information (Figure S4, Supporting Information).

doses. Based on the above results (from Figure 4 to Figure 7), it can be summarized that siRNA-encapsulated nanoparticles with $ScFv_{Her2}$ decoration enhanced cellular uptake by receptor-mediated endocytosis in $Her2^+$ breast cancer cells, thus improving Plk1 gene downregulation and subsequently inhibiting cell proliferation and elevating cell apoptosis.

2.6. $ScFv_{Her2}$-NP_{siPlk1} Improved siRNA Accumulation and Enhanced Tumor Cell Uptake in $Her2^+$ Breast Cancer Xenograft

The $ScFv_{Her2}$ on the surface of $ScFv_{Her2}$-NP_{siRNA} can specifically bind to $Her2^+$ breast tumor cells, and then enhance the uptake of $ScFv_{Her2}$-NP_{siRNA} into $Her2^+$ breast tumor cells via receptor-mediated endocytosis. In contrast, NP_{siRNA} was less readily internalized but more easily eliminated by the lymphatic system.[32] Thus, we speculated that with $ScFv_{Her2}$ decoration, $ScFv_{Her2}$-NP_{siRNA} could improve siRNA accumulation and enhance tumor cell uptake in vivo. In order to verify this, we performed fluorescence imaging at predetermined time points after the intravenous injection of different formulations into a mouse bearing a $Her2^+$ BT474 xenograft. As shown in **Figure 8**A, the in vivo fluorescence distribution in tumor-bearing mice was detected at 1, 2, 4, and 24 h after administering free Cy5-siRNA, $ScFv_{Her2}$-$NP_{Cy5\text{-}siRNA}$, or nontargeted $NP_{Cy5\text{-}siRNA}$. The fluorescence intensity from $ScFv_{Her2}$-$NP_{Cy5\text{-}siRNA}$ in the subcutaneous tumor site was significantly higher than that from nontargeted nanoparticles at all time points after injection. Quantitative analysis was further conducted to verify the imaging results (Figure 8B,C). At 4 h or 24 h post-injection, the mice were sacrificed and major organs such as the heart, lungs, liver, spleen, and kidneys, and the tumor was excised to analyze the in vivo distribution of Cy5-siRNA. Compared with the nontargeted $NP_{Cy5\text{-}siRNA}$, the accumulation of Cy5-siRNA in tumor tissue was increased by 2.07 times at 4 h and 1.55 times at 24 h post-injection of $ScFv_{Her2}$-$NP_{Cy5\text{-}siRNA}$. The data were consistent with the in vivo imaging results, indicating that more siRNA delivered by $ScFv_{Her2}$-NP accumulated in tumor tissues than siRNA delivered by nontargeted NP. In addition, the $ScFv_{Her2}$-NP group and the nontargeted NP group showed no significant differences in their distribution in major organs.

2.7. $ScFv_{Her2}$-NP_{siPlk1} Significantly Promoted an Anti-Tumor Effect Following Intravenous Injection

The enhanced delivery of siRNA to $Her2^+$ tumor cells via $ScFv_{Her2}$-NP could potentially enhance the efficiency of siRNA in cancer therapy in vivo. To evaluate this, we examined the anti-tumor effect in mice with $Her2^+$ BT474 or $Her2^-$ MDA-MB-231 xenografts by intravenous injection of different formulations at a siRNA dose of 20 μg per injection from 14 d post-xenograft implantation. Blank nanoparticles ($ScFv_{Her2}$-NP or non-target NP) without siRNA encapsulation, $ScFv_{Her2}$-$NP_{siN.C}$, and free si*Plk1* were used as negative controls. As illustrated in **Figure 9**A, in $Her2^+$ BT474 and $Her2^-$ MDA-MB-231 xenografts, treatment with the free si*Plk1*, blank nanoparticles, and $ScFv_{Her2}$-$NP_{siN.C.}$ did not show tumor growth inhibition in comparison with PBS. In $Her2^+$ BT474 xenografts, the delivery of si*Plk1* with $ScFv_{Her2}$-NP or nontargeted nanoparticles could

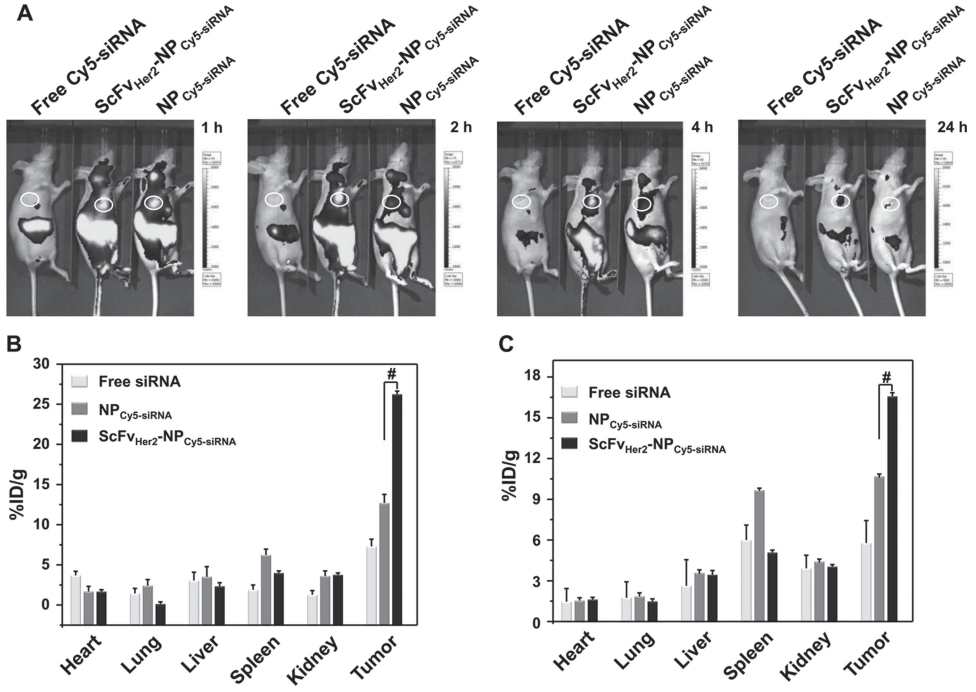

Figure 8. A) Fluorescence images of $Her2^+$ BT474 xenograft-bearing mice after intravenous (i.v.) injection of free Cy5-siRNA, $ScFv_{Her2}$-$NP_{Cy5\text{-}siRNA}$, or nontargeted $NP_{Cy5\text{-}siRNA}$. The tumor sites are labeled with green circles. B,C) Biodistribution of Cy5-siRNA in $Her2^+$ BT474 xenograft-bearing mice after receiving i.v. injection of free Cy5-siRNA, $ScFv_{Her2}$-$NP_{Cy5\text{-}siRNA}$, or nontargeted $NP_{Cy5\text{-}siRNA}$ at 4 h (B) and 24 h (C). The dose of Cy5-siRNA was 3.0 nmol per mouse. $^{\#}p < 0.01$ when compared with $NP_{Cy5\text{-}siRNA}$ ($n = 3$).

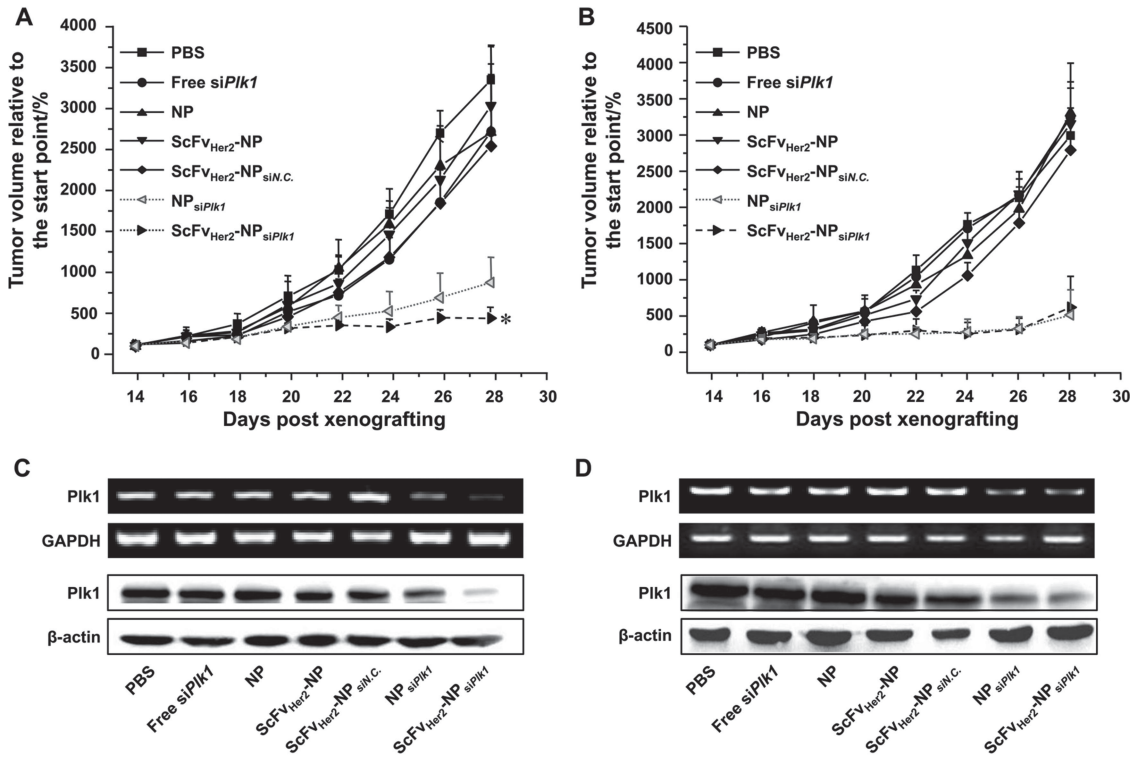

Figure 9. A,B) Inhibition of tumor growth in a murine model with Her2$^+$ BT474 xenografts (A) and Her2$^-$ MDA-MB-231 xenografts (B) after treatment with different formulations. * $p < 0.05$ when compared with NP$_{siPlk1}$ ($n = 6$). C,D) Expression of Plk1 mRNA and protein in Her2$^+$ BT474 tumor and Her2$^-$ MDA-MB-231 tumor analyzed 24 h after the last injection. The mice bearing tumors received one intravenous injection every other day from the 14th day post- xenograft implantation in all of the experiments. ScFv$_{Her2}$-NP (or NP), ScFv$_{Her2}$-NP$_{siN.C.}$, and ScFv$_{Her2}$-NP$_{siPlk1}$ (or NP$_{siPlk1}$) represent mice administered with blank nanoparticles ScFv$_{Her2}$-NP (or empty nanoparticles NP) and ScFv$_{Her2}$-NP (or nontargeted NP) carrying si$_{N.C.}$ or si*Plk1*, respectively. The dose of siRNA was 20 μg per mouse per injection.

efficiently inhibit tumor growth in the murine model, while the delivery of si*Plk1* with ScFv$_{Her2}$-NP showed an enhanced inhibition of tumor growth compared with the nontargeted nanoparticle group. In contrast, in Her2$^-$ MDA-MB-231 xenografts, the delivery of si*Plk1* with ScFv$_{Her2}$-NP or nontargeted nanoparticles exhibited a similar inhibition of tumor growth (Figure 9B).

To further evaluate whether enhanced inhibition of tumor growth by ScFv$_{Her2}$-NP$_{siPlk1}$ in Her2$^+$ BT474 xenografts was related to improved Plk1 gene silencing, Plk1 expression at the mRNA and protein levels in the tumors was analyzed by RT-PCR and Western blot analyses following the treatment. As shown in Figure 9C,D, compared with mice treated with nontargeted NP$_{siPlk1}$, those treated with ScFv$_{Her2}$-NP$_{siPlk1}$ showed enhanced downregulation of Plk1 gene expression at both the mRNA and protein levels in Her2$^+$ BT474 xenografts, whereas similar downregulation efficiencies were observed in Her2$^-$ MDA-MB-231 xenografts.

In Figure 9A, ScFv$_{Her2}$ decoration statistically enhanced inhibition of Her2$^+$ tumor growth, but the antitumor efficiency of ScFv$_{Her2}$-NP$_{siPlk1}$ at 20 μg per injection did not show remarkable difference compared with the nontargeted nanoparticles at the same siRNA dose. Therefore, a dose-dependent antitumor response was observed for ScFv$_{Her2}$-NP$_{siPlk1}$ and NP$_{siPlk1}$ in Her2$^+$ BT474 xenografts. The mice bearing Her2$^+$ BT474 received intravenous injection of different siRNA doses per injection from 14-d post xenograft implantation. As shown in **Figure 10**, treatment with nontargeted NP$_{siPlk1}$ at a dose of 20 μg per injection inhibited tumor growth, but when the dose was reduced to 10 μg per injection, only moderate inhibition of tumor growth was observed. On the contrary, ScFv$_{Her2}$-NP$_{siPlk1}$ at a dose of 10 μg per injection efficiently inhibited tumor growth; the level of inhibition was better than the anticancer effect of treatment with nontargeted nanoparticles at a dose of 20 μg per injection, indicating that ScFv$_{Her2}$ decoration significantly enhanced the inhibition of tumor growth and efficiently reduced the siRNA dose in Her2$^+$ BT474 xenografts.

3. Conclusion

Enhanced in vivo siRNA delivery efficiency is desirable for clinical application. Here, we developed ScFv$_{Her2}$-decorated PEG-PLA-based nanoparticles for tumor-targeted siRNA delivery. We demonstrated that ScFv$_{Her2}$-NP$_{siRNA}$ could specifically bind to the Her2 antigen, which is overexpressed on the surface of breast cancer cells. Accordingly, improved uptake by tumor cells, increased silencing efficiency, and enhanced tumor cell apoptosis were observed. More importantly, ScFv$_{Her2}$-NP$_{siRNA}$ enhanced tumor accumulation of siRNA in a mouse model bearing Her2$^+$ breast tumor xenograft, as assessed by in vivo fluorescence imaging and quantitative siRNA analyses. Besides,

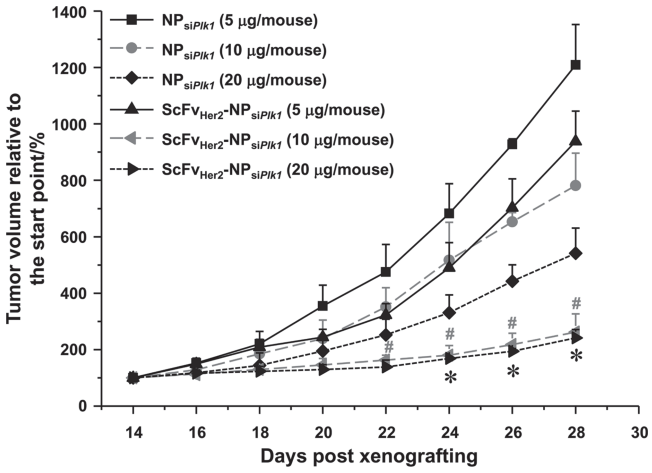

Figure 10. Inhibition of tumor growth in the murine model with Her2$^+$ BT474 xenografts after treatment with different formulations. The mice bearing tumors received one intravenous injection every other day from the 14th day post xenograft implantation in all of the experiments. ScFv$_{Her2}$-NP$_{siPlk1}$ and NP$_{siPlk1}$ represent mice administered with ScFv$_{Her2}$-NP or nontargeted NP carrying si*Plk1*, respectively. The dose of siRNA was 5 μg, 10 μg, or 20 μg per mouse per injection. * $p < 0.05$ when compared with NP$_{siPlk1}$ at a siRNA dose of 20 μg per mouse per injection ($n = 6$). $^{\#}p < 0.05$ when compared with NP$_{siPlk1}$ at a siRNA dose of 10 μg per mouse per injection ($n = 6$).

ScFv$_{Her2}$-NP$_{siRNA}$ significantly improved the efficacy of tumor suppression and substantially reduced the dose of injected siRNA compared with nontargeted nanoparticles, indicating that the ScFv$_{Her2}$-decorated nanoparticle shows great potential for targeted RNA interference therapy of Her2$^+$ breast tumor.

4. Experimental Section

Materials: The cationic lipid *N*,*N*-bis(2-hydroxyethyl)-*N*-methyl-*N*-(2-cholesteryloxycarbonyl aminoethyl) ammonium bromide (BHEM-Chol), methoxy-terminated poly(ethylene glycol)-block-poly(D,L-lactide) copolymer (mPEG$_{5k}$-PLA$_{10K}$), and maleimide-terminated poly(ethylene glycol)-block-poly(D,L-lactide) (Mal-PEG$_{5k}$-PLA$_{21K}$) were prepared as previously described.[14,33] Poly(vinyl alcohol) (PVA, 88% hydrolyzed, Mw = 22 000) was purchased from Acros Organics Co. (Morris Plains, NJ). Other organic solvents or reagents were of analytic grade and used as received. Ultra-purified water was prepared using a Milli-Q Synthesis System (Millipore, Bedford, MA, USA). Dulbecco's modified Eagle's medium (DMEM) and L-glutamine were purchased from Gibco BRL (Eggenstein, Germany). The Lipofectamine 2000 transfection kit from Invitrogen (Carlsbad, USA) was used as suggested by the supplier. Fluorescently labeled FAM-siRNA and Cy5-siRNA, negative control siRNA with a scrambled sequence (si*N.C.*, antisense strand, 5′-ACGUGACACGUUCGGAGAAdTdT-3′) and siRNA targeting the Plk1 mRNA (si*Plk1*, antisense strand, 5′-UAAGGAGGGUGAUCUUCUUCAdTdT-3′) were synthesized by Suzhou Ribo Life Science Co. (Kunshan, China).

Preparation of Recombinant Protein ScFv$_{Her2}$ with a C-Terminal Cysteine: The expression cassette encoding ScFv$_{Her2}$ followed by a C-terminal hexahistidine tag and then cysteine was amplified by polymerase chain reaction (PCR) using the plasmid pAcGP67B-ScFv$_{Her2}$ as a template.[34] The forward and reverse primers (Sangon Biotech, China) were 5′-CATGccatggTGATGGCCCAGGTGCAGCTGGTG-3′ and 5′-CCGctcgagTTAACAATGGTGGTGGTGATGATGAGATCC-3′, containing the restriction sites for NcoI and XhoI, respectively. The reverse primer also contained the reverse-complement sequence of a C-terminal hexahistidine tag and followed by cysteine. The PCR-amplified DNA fragment was purified, digested with NcoI and XhoI, and ligated into pET28a (+) vector (Novagen, Madison, WI, USA). The recombinant plasmid pET28a- ScFv$_{Her2}$-Cys was verified by sequencing. The pET28a-ScFv$_{Her2}$-Cys plasmid was transformed into *Escherichia coli* strain BL21 (DE3). The expression of recombinant ScFv$_{Her2}$-Cys protein was performed in 10 L Luria Bertani broth cultures medium containing 50 mg L^{-1} kanamycin, which was incubated at 37 °C until OD$_{600}$ of the culture reached about 0.6. Expression was induced by the addition of 1×10^{-3} M isopropyl β-D-thiogalactopyranoside (IPTG, Sigma-Aldrich, St. Louis, USA) for an additional 4 h at 37 °C. For the preparation of soluble protein fractions, cells from 10 L culture were first pelleted and then resuspended in 300 mL cold lysis buffer containing 50×10^{-3} M Tris-HCl pH 8.0, 200×10^{-3} M NaCl, 5% glycerol, and 5×10^{-3} M imidazole (Sigma-Aldrich). The cell suspension was then passed through a French Press cell disruptor three times followed by centrifugation at 48 000 *g* for 30 min. The clear supernatant containing soluble protein was collected by centrifugation. All the following purification steps were performed at 4 °C. Recombinant ScFv$_{Her2}$-Cys with a C-terminal hexahistidine tag was purified using Ni-NTA His-bind resin (Novagen). Once all unbound proteins had been washed from the column using 50×10^{-3} M Tris-HCl pH 8.0, 200×10^{-3} M NaCl, 5% glycerol, and 20×10^{-3} M imidazole, recombinant ScFv$_{Her2}$-Cys protein was eluted from the column using 250×10^{-3} M imidazole along with 50×10^{-3} M Tris-HCl pH 8.0, 200×10^{-3} M NaCl, and 5% glycerol. Finally, the eluted protein was changed into PBS buffer using a PD-10 desalting column (GE Healthcare, Piscataway, NJ, USA) and further purified with a size exclusion column (HiLoad 16/60 Superdex 200; Amersham Biosciences, Sweden). Recombinant ScFv$_{Her2}$ protein was obtained with a final yield of 0.5 mg per liter of cell culture. The purity of the protein was estimated using SDS-PAGE, and then stained with Coomassie Blue.

Enzyme-Linked Immunosorbent Assay (ELISA): Ninety-six-well plates were coated with 100 μL cell lysates from Her2$^+$ BT474 cancer cells (0.1 mg mL^{-1}) in PBS overnight at 37 °C, and blocked for 2 h with 5% bovine serum albumin (BSA, Sangon Biotech, China) in PBS. The ScFv$_{Her2}$ and His-tagged Her2 monoclonal antibody (a gift from Prof. J Liu, University of Science and Technology of China) were added to coated ELISA plates and allowed to bind for 2 h at 37 °C. Plates were rinsed with PBS/0.1% Tween 20, and anti-His×6 tag antibody was added to the plates in PBS and allowed to bind for 2 h. Plates were washed and goat anti-mouse IgG-HRP (sc-2302, Santa Cruz Biotechnology Inc., CA, USA) diluted 1:5000 in PBS, 50 μL well^{-1}, was added and incubated for 1 h at room temperature. Plates were washed four times and developed with 75 μL 3,3′,5,5′-tetramethylbenzidine (TMB; Sigma-Aldrich) reagent and the reaction was stopped with 75 μL HCL (1.0 M). Plates were measured at 450 nm using a plate reader.

Preparation of ScFv$_{Her2}$-Decorated Nanoparticles with siRNA Encapsulation (ScFv$_{Her2}$-NP$_{siRNA}$) and Nontargeted Nanoparticles (NP$_{siRNA}$): Nanoparticles encapsulating siRNA were prepared by a double-emulsion solvent evaporation technique as previously described.[14] To prepare this nanoparticle, an aqueous solution of siRNA (0.2 mg, 15 nmol) in 25 μL of RNase-free water was emulsified by sonication for 30 s over an ice bath in 0.5 mL of chloroform containing 1.0 mg of BHEM-Chol, 2.5 mg of Mal-PEG$_{5k}$-PLA$_{21k}$, and 22.5 mg of mPEG$_{5K}$-PLA$_{10K}$. This primary emulsion was further emulsified in 1.5 mL of PVA solution (1.0%, w/v) by sonication (80 W for 2 min) over an ice bath to form a water-in-oil-in-water emulsion. The mixture was then added to 25 mL of PVA solution (0.3%, w/v), which was further stirred for 3 h to allow the evaporation of chloroform. The particles were collected by centrifugation (30 000 g, 1 h) and washed twice with sterile water to remove PVA and possible un-encapsulated siRNA. The supernatant was also collected for encapsulation efficiency analyses as previously described.[14] This siRNA-loaded nanoparticle formulation was further denoted as Mal-NP$_{siRNA}$. To prepare ScFv$_{Her2}$-NP$_{siRNA}$, ScFv$_{Her2}$-Cys was chemically conjugated onto the surface of Mal-NP$_{siRNA}$ through a covalent thiol-maleimide linkage at equal molar ratio. The reaction was carried out in 0.1 M phosphate buffer (PB), pH 6.8 and incubated at 37 °C for 12 h. Subsequently, the reaction solution was centrifuged at 30 000 *g* for 1 h; the supernatant

was collected and analyzed by SDS-PAGE followed by Coomassie Blue staining, and the supernatant from the mixture of $ScFv_{Her2}$-Cys and Mal-NP_{siRNA} without incubation was used as the control. The formation of the thioether bond between nanoparticles and $ScFv_{Her2}$-Cys was characterized with Ellman's Reagent (5,5′-dithiobis-2-nitrobenzoic acid [DTNB], Sigma-Aldrich) according to the literature.[35] The collected nanoparticles were suspended in ultra-purified water, and the unreacted maleimide groups were quenched by adding L-cysteine (biochemical reagent, Shanghai, China) to obtain $ScFv_{Her2}$-decorated nanoparticles with siRNA encapsulation ($ScFv_{Her2}$-NP_{siRNA}). In addition, the control nontargeted nanoparticles encapsulating siRNA (NP_{siRNA}) were prepared by reacting the maleimide groups of Mal-NP_{siRNA} with L-cysteine. The reaction also was carried out in 0.1 M phosphate buffer (PB), pH 6.8, and incubated at 37 °C for 12 h as described above.

Characterization of $ScFv_{Her2}$-NP_{siRNA}: The average diameter of $ScFv_{Her2}$-NP_{siRNA} in water was analyzed by a Zetasizer Nano ZS90 apparatus (Malvern, UK) at 25 °C, by illuminating the sample with 633 nm wavelength radiation from a solid-state He–Ne laser and collecting the scattered light at an angle of 90°. The nanoparticles were analyzed in triplicate at a concentration of 1.0 mg mL^{-1}. The morphology of $ScFv_{Her2}$-NP_{siRNA} was analyzed by JEOL-2010 TEM at an accelerating voltage of 200 kV.

Cell Culture: The human breast cancer cell line BT474 ($Her2^+$) and MDA-MB-231 ($Her2^-$) from the American Type Culture Collection (ATCC) were maintained in DMEM supplemented with 10% FBS (Hyclone, Waltham, USA), 4×10^{-3} M L-glutamine, and 1% penicillin/streptomycin (Sigma-Aldrich). Cells were incubated at 37 °C in a 5% CO_2 atmosphere.

Cellular Uptake of $ScFv_{Her2}$-NP_{siRNA}: For flow cytometric analysis, $Her2^+$ BT474 and $Her2^-$ MDA-MB-231 cells were seeded onto 24-well plates at 5.0×10^4 cells per well in 0.5 mL complete DMEM medium and cultured at 37 °C in a 5% CO_2 humidified atmosphere for 24 h. The medium was replaced with complete DMEM medium containing free FAM-siRNA, $ScFv_{Her2}$-$NP_{FAM\text{-}siRNA}$, or $NP_{FAM\text{-}siRNA}$. The final concentration of FAM-siRNA in the culture medium was 50×10^{-9} M. The cells were incubated at 37 °C for 1 h, and then rinsed twice with cold PBS. The cells were trypsinized, washed with cold PBS (pH 7.4), filtered through a 35-μm nylon mesh, and subjected to flow cytometric analysis using a BD FACS Calibur flow cytometer (BD Bioscience, Bedford, MA, USA). The results were analyzed using WinMDI 2.9 software (The Scripps Research Institute, La Jolla, CA). In the competitive inhibition assay, free $ScFv_{Her2}$-Cys (100×10^{-9} M) was pre-incubated with $Her2^+$ BT474 cells 1 h before the addition of $ScFv_{Her2}$-$NP_{FAM\text{-}siRNA}$. To analyze the internalization of nanoparticles, $Her2^+$ BT474 cells (1×10^5 cells $well^{-1}$) were seeded on coverslips on a 24-well plate and incubated for 24 h. The medium was replaced with complete DMEM medium containing $ScFv_{Her2}$-$NP_{Cy5\text{-}siRNA}$ or nontargeted $NP_{Cy5\text{-}siRNA}$ as described above. After 1 h of incubation, the cells were washed twice with PBS, and fixed with ice-cold ethanol, then blocked using 1% BSA (Sangon Biotech, China) in PBS for 20 min. Then, the cells were incubated with mouse monoclonal anti-ErbB2 antibody (1:1000, sc-33684, Santa Cruz Biotechnology Inc.) for 30 min at 37 °C, washed repeatedly to remove the excess antibody, and incubated with goat anti-rabbit IgG-FITC (Santa Cruz Biotechnology Inc.) for 30 min. After washing twice with PBS, the cells were counterstained with DAPI (Sigma-Aldrich) according to the standard protocol provided by the suppliers. Coverslips were mounted on glass microscope slides with a drop of anti-fade mounting media (Sigma-Aldrich) to reduce fluorescence photobleaching. The cellular distribution of nanoparticles was visualized by a confocal laser scanning microscope (LSM 710, Carl Zeiss Inc., Germany).

In Vitro Transfection and Analysis of Gene Expression: $Her2^+$ BT474 and $Her2^-$ MDA-MB-231 were seeded on six-well plates (2.0×10^5 per well) and allowed to grow until 50% confluence. The cells were treated for 24 h with different formulations, including PBS, free si*Plk1* at 200×10^{-9} M, the blank nontargeted NP or $ScFv_{Her2}$-NP (without siRNA encapsulation) at a concentration of 0.36 mg mL^{-1}, and $ScFv_{Her2}$-$NP_{siN.C.}$ at a polymer concentration of 0.36 mg mL^{-1} and the corresponding concentration of si*N.C.* at 200×10^{-9} M as the controls. Lipofectamine 2000 carrying 50×10^{-9} M of si*Plk1* was also used as the positive control. In the treatments with $ScFv_{Her2}$-NP_{siPlk1}, the polymer concentrations were varied from 0.09 to 0.36 mg mL^{-1}, while the corresponding concentrations of si*Plk1* were from 50×10^{-9} to 200×10^{-9} M. After further incubation for 36 h (for mRNA isolation) or 72 h (for protein extraction) at 37 °C, the cellular levels of Plk1 mRNA and protein were assessed using RT-PCR and Western blotting, respectively. In RT-PCR analysis, the cells were collected and total RNA from transfected cells was isolated using an RNeasy mini-kit (Qiagen, Shanghai, China) according to the protocol of the manufacturer. Two micrograms of total RNA was transcribed into complementary DNA (cDNA) using the PrimeScript first Strand cDNA Synthesis Kit (Takara, Dalian, China). Thereafter, 2 μL of cDNA was subjected to PCR analysis targeting Plk1 and glyceraldehyde 3-phosphate dehydrogenase (GAPDH; Takara, Dalian, China). The primers used in the PCR for Plk1 and GAPDH were: 5′-AGCCTGAGGCCCGATACTACCTAC-3′ (Plk1-forward), 5′-ATTAGGAGTCCCACACAGGGTCTTC-3′ (Plk1-reverse), 5′-TTCACCACCATGGAGAAGGC-3′ (GAPDH-forward), and 5′-GGCATGGACTGTGGTCATGA-3′ (GAPDH-reverse). PCR parameters consisted of 30 s of *rTaq* activation at 95 °C, followed by 30 cycles of PCR at 95 °C ×5 s, 55 °C ×30 s, and 72 °C ×30 s. In Western blot analysis, transfected cells were first washed twice with cold PBS, and then resuspended in 50 μL of lysis buffer (50×10^{-3} M HEPES, pH 7.5, 150×10^{-3} M NaCl, 1% Triton X-100, 10% glycerol, 1.5×10^{-3} M $MgCl_2$, 1×10^{-3} M EGTA) freshly supplemented with Complete Protease Inhibitor Cocktail Tablets (Roche, Basel, Switzerland). The cell lysates were incubated on ice for 1 h and vortexed every 5 min. The lysates were then clarified by centrifugation for 10 min at 12 000 *g*. The protein concentration was determined using the BCA Protein Assay Kit (Lot: 23250, Thermo, USA). Total protein (100 μg) was separated on 12% Bis-Tris-polyacrylamide gels and then transferred (at 300 mA for 45 min) to Immobilon-P membranes (Millipore, Bedford, MA, USA). After incubation in 5% BSA in PBS with Tween-20 (PBST; pH 7.2) for 2 h, the membranes were incubated in 1% BSA in PBS with monoclonal antibodies against Plk1 (1:1000) overnight. After incubation in 1% BSA with goat anti-mouse IgG-HRP antibody (1:10,000) for 30 min, bands were visualized using ImageQuant LAS 4000 mini (GE Healthcare).

Cell Viability Assay and Cell Apoptosis Analysis: For cell viability assay, $Her2^+$ BT474 and $Her2^-$ MDA-MB-231 cells were seeded onto 96-well plates (2.0×10^3 per well) and allowed to grow until 50% confluence. The cells were treated with the above-mentioned formulations. After 72 h of treatment, MTT (Sigma-Aldrich) stock solution was added to each well to achieve a final concentration of 1 g L^{-1}, with the exception of the wells used as a blank, to which the same volume of PBS (0.01 M, pH 7.4) was added. After incubation for an additional 2 h, 100 μL of the extraction buffer (20% SDS in 50% *N*,*N*-dimethylformamide, pH 4.7, prepared at 37 °C) was added to the wells and incubated overnight at 37 °C. The absorbance was measured at 570 nm using a Bio-Rad 680 microplate reader (Bio-Red, USA). Cell viability was normalized to that of cells cultured in the culture medium with PBS treatment. For cell apoptosis analysis, $Her2^+$ BT474 and $Her2^-$ MDA-MB-231 cells were seeded onto 24-well plates and allowed to grow until 50% confluence. The cells were treated with the above-mentioned formulations. After 72 h of treatment, the cells were collected and apoptotic cells were detected by flow cytometry after treatment with the Annexin V-FITC apoptosis detection kit I (BD Biosciences) according to the suggested procedure. The results were analyzed using WinMDI 2.9 software.

Animal Models: BALB/c nude mice (6 weeks old) were purchased from the Shanghai Experimental Animal Centre of the Chinese Academy of Sciences (Shanghai, China) and all animals received care in compliance with the guidelines outlined in the Guide for the Care and Use of Laboratory Animals. The procedures were approved by the University of Science and Technology of China Animal Care and Use Committee. The xenograft tumor model was generated by subcutaneous injection of $Her2^+$ BT474 cells (1×10^6 for each mouse) or $Her2^-$ MDA-MB-231 (2×10^6 for each mouse) in the mammary fat pad of the mouse. At 14 days after tumor cell implantation, the tumor volume was about 60 mm^3 and 50 mm^3 for $Her2^+$ BT474 and $Her2^-$ MDA-MB-231 tumor model, respectively, and the mice were used for the subsequent experiments.

Distribution of siRNA In Vivo: Her2$^+$ BT474 tumor-bearing mice were intravenously injected with 200 μL of $ScFv_{Her2}$-$NP_{Cy5\text{-}siRNA}$ or $NP_{Cy5\text{-}siRNA}$, containing 40 μg Cy5-siRNA (3.0 nmol), or free Cy5-siRNA (3.0 nmol). The mice were anesthetized at the predetermined time points, and imaged by a Xenogen IVIS Lumina system (Caliper Life Sciences, USA). The results were analyzed using Living Image 3.1 software (Caliper Life Sciences). Then, the mice (three mice per group) were sacrificed and the organs (tumor, heart, liver, spleen, kidney, and lung) were excised and homogenized for quantitative assay as we previous reported.[36]

Tumor Suppression Study: Her2$^+$ BT474 or Her2$^-$ MDA-MB-231 tumor-bearing mice were randomly divided into seven groups (six mice per group), and treated with PBS, free si*Plk1*, blank $ScFv_{Her2}$-NP and NP without siRNA encapsulation, NP_{siPlk1}, $ScFv_{Her2}$-$NP_{siN.C.}$, or $ScFv_{Her2}$-NP_{siPlk1} by intravenous injection once every other day. The dose of siRNA for free si*Plk1*, NP_{siPlk1}, $ScFv_{Her2}$-$NP_{siN.C.}$, and $ScFv_{Her2}$-NP_{siPlk1} was 20 μg (1.5 nmol) per mouse per injection, and the dose of blank nanoparticles without siRNA encapsulation ($ScFv_{Her2}$-NP and NP) was 2.71 mg per mouse per injection. Tumor growth was monitored by measuring the perpendicular diameter of the tumor using calipers. The estimated volume was calculated according to the following formula: tumor volume (mm^3) = 0.5 × length × width^2. One day after the last injection, the animals were sacrificed and the tumors were excised for RT-PCR and Western blot analyses. To further demonstrate the advantage of $ScFv_{Her2}$ decoration, dose-dependent anti-tumor response was assessed for $ScFv_{Her2}$-NP_{siPlk1} and NP_{siPlk1} in the Her2$^+$ BT474 tumor model. To obtain tumor model possessed similar tumor size, a solid tumor tissue (about 1500 mm^3) was harvested from a mouse bearing an MDA-MB-231 xenograft, and cut into small fragments (ca. 3 mm). Then, the fragment of tumor tissue was implanted in the mammary fat pad of the mouse to generate Her2$^+$ BT474 xenograft tumor model. The Her2$^+$ BT474 tumor-bearing mice were randomly divided into six groups (six mice per group), and treated with $ScFv_{Her2}$-NP_{siPlk1} or NP_{siPlk1} at different doses of siRNA (5 μg, 10 μg, and 20 μg per mouse per injection) by intravenous injection once every other day. Tumor growth was monitored by measuring the perpendicular diameter of the tumor using calipers as described above.

Detection of Plk1 Expression in Tumor Tissue: For Plk1 mRNA analysis, tumor tissues were collected and lysed using an RNeasy mini-kit. The mRNA was collected and analyzed by RT-PCR as describe above. To determine Plk1 protein expression in tumor tissue after treatments, tumor tissues were collected and lysed in 100 μL tissue lysis buffer (50×10^{-3} M HEPES, pH 7.5, 150×10^{-3} M NaCl, 1×10^{-3} M EGTA, 2.5×10^{-3} M ethylenediaminetetraacetic acid (EDTA) 10% glycerol, 0.1% Tween 20, 1×10^{-3} M dithiothreitol, 10×10^{-3} M glycerol 2-phosphate, 1×10^{-3} M NaF, and 0.1×10^{-3} M Na_3VO_4) freshly supplemented with Roche's Complete Protease Inhibitor Cocktail Tablets. The lysates were incubated on ice for a total of 30 min and vortexed every 5 min. The lysates were centrifuged for 10 min at 12 000 *g*. Then the protein was detected by Western blot analyses as describe above.

Statistical Analysis: Statistical analyses were performed using Student's *t-test* to measure statistical differences among groups. Data with $p < 0.05$ were considered to be statistically significant.

Supporting Information

Supporting Information is available from the Wiley Online Library or from the author.

Acknowledgements

This work was supported by the National Basic Research Program of China (973 Programs, 2010CB934001), the National High Technology Research and Development Program of China (863 Program 2014AA020708), the National Natural Science Foundation of China (51203145, 51390482, 81172526, 81302724), Anhui Provincial Natural Science Foundation (1308085QB26), the Fundamental Research Funds for the Central Universities (2014HGCH0014, 2013HGCH0001) and China Postdoctoral Science Foundation (2012M511407, 2013T60614, 2012M521258).

Received: January 15, 2014
Revised: March 31, 2014
Published online: June 20, 2014

[1] R. Siegel, D. Naishadham, A. Jemal, *CA Cancer J. Clin.* **2012**, *62*, 10.
[2] D. J. Slamon, G. M. Clark, S. G. Wong, W. J. Levin, A. Ullrich, W. L. McGuire, *Science* **1987**, *235*, 177.
[3] a) C. Wright, B. Angus, S. Nicholson, J. R. Sainsbury, J. Cairns, W. J. Gullick, P. Kelly, A. L. Harris, C. H. Horne, *Cancer Res.* **1989**, *49*, 2087; b) M. Piccart, C. Lohrisch, A. Di Leo, D. Larsimont, *Oncology* **2001**, *61*, 73.
[4] a) R. Rouzier, C. M. Perou, W. F. Symmans, N. Ibrahim, M. Cristofanilli, K. Anderson, K. R. Hess, J. Stec, M. Ayers, P. Wagner, P. Morandi, C. Fan, I. Rabiul, J. S. Ross, G. N. Hortobagyi, L. Pusztai, *Clin. Cancer Res.* **2005**, *11*, 5678; b) J. S. Parker, M. Mullins, M. C. U. Cheang, S. Leung, D. Voduc, T. Vickery, S. Davies, C. Fauron, X. He, Z. Hu, J. F. Quackenbush, I. J. Stijleman, J. Palazzo, J. S. Marron, A. B. Nobel, E. Mardis, T. O. Nielsen, M. J. Ellis, C. M. Perou, P. S. Bernard, *J. Clin. Oncol.* **2009**, *27*, 1160.
[5] C. L. Arteaga, M. X. Sliwkowski, C. K. Osborne, E. A. Perez, F. Puglisi, L. Gianni, *Nat. Rev. Clin. Oncol.* **2012**, *9*, 16.
[6] K. L. Jones, A. U. Buzdar, *Lancet Oncol.* **2009**, *10*, 1179.
[7] a) K. Strebhardt, A. Ullrich, *Nat. Rev. Cancer* **2006**, *6*, 321; b) Y. Degenhardt, T. Lampkin, *Clin. Cancer Res.* **2010**, *16*, 384; c) K. C. Goh, H. S. Wang, N. F. Yu, Y. F. Zhou, Y. Zheng, Z. Y. Lim, K. Sangthongpitag, L. J. Fang, M. Du, X. K. Wang, A. B. Jefferson, J. Rose, B. Shamoon, C. Reinhard, B. Carte, M. Entzeroth, B. H. Ni, M. L. Taylor, W. Stunkel, *Drug Dev. Res.* **2004**, *62*, 349; d) N. Takai, R. Hamanaka, J. Yoshimatsu, I. Miyakawa, *Oncogene* **2005**, *24*, 287.
[8] B. Spankuch, I. Steinhauser, H. Wartlick, E. Kurunci-Csacsko, K. I. Strebhardt, K. Langer, *Neoplasia* **2008**, *10*, 223.
[9] a) X. Q. Liu, R. L. Erikson, *Proc. Natl. Acad. Sci. U.S.A.* **2003**, *100*, 5789; b) A. D. Judge, M. Robbins, I. Tavakoli, J. Levi, L. Hu, A. Fronda, E. Ambegia, K. McClintock, I. MacLachlan, *J. Clin. Invest.* **2009**, *119*, 661.
[10] a) C. McInnes, M. D. Wyatt, *Drug Discovery Today* **2011**, *16*, 619; b) S. Lapenna, A. Giordano, *Nat. Rev. Drug Discovery* **2009**, *8*, 547.
[11] R. D. Hofheinz, S. E. Al-Batran, A. Hochhaus, E. Jaeger, V. L. Reichardt, H. Fritsch, D. Trommeshauser, G. Munzert, *Clin. Cancer Res.* **2010**, *16*, 4666; b) D. Olmos, D. Barker, R. Sharma, A. T. Brunetto, T. A. Yap, A. B. Taegtmeyer, J. Barriuso, H. Medani, Y. Y. Degenhardt, A. J. Allred, D. A. Smith, S. C. Murray, T. A. Lampkin, M. M. Dar, R. Wilson, J. S. de Bono, S. P. Blagden, *Clin. Cancer Res.* **2011**, *17*, 3420; c) D. D. Von Hoff, C. Taylor, S. Rubin, J. Cohen, L. Garland, *J. Clin. Oncol.* **2004**, *22*, 203S.
[12] a) J. D. Heidel, Z. Yu, J. Y. C. Liu, S. M. Rele, Y. Liang, R. K. Zeidan, D. J. Kornbrust, M. E. Davis, *Proc. Natl. Acad. Sci. U.S.A.* **2007**, *104*, 5715; b) M. E. Davis, J. E. Zuckerman, C. H. J. Choi, D. Seligson, A. Tolcher, C. A. Alabi, Y. Yen, J. D. Heidel, A. Ribas, *Nature* **2010**, *464*, 1067; c) P. Kumar, H. S. Ban, S. S. Kim, H. Wu, T. Pearson, D. L. Greiner, A. Laouar, J. Yao, V. Haridas, K. Habiro, Y. G. Yang, J. H. Jeong, K. Y. Lee, Y. H. Kim, S. W. Kim, M. Peipp, G. H. Fey, N. Manjunath, L. D. Shultz, S. K. Lee, P. Shankar, *Cell* **2008**, *134*, 577; d) D. Peer, E. J. Park, Y. Morishita, C. V. Carman, M. Shimaoka, *Science* **2008**, *319*, 627; e) P. Resnier, T. Montier, V. Mathieu, J. P. Benoit, C. Passirani, *Biomaterials* **2013**, *34*, 6429.

[13] a) T. M. Sun, J. Z. Du, Y. D. Yao, C. Q. Mao, S. Dou, S. Y. Huang, P. Z. Zhang, K. W. Leong, E. W. Song, J. Wang, *ACS Nano* **2011**, *5*, 1483; b) X. Z. Yang, S. Dou, Y. C. Wang, H. Y. Long, M. H. Xiong, C. Q. Mao, Y. D. Yao, J. Wang, *ACS Nano* **2012**, *6*, 4955; c) X. Z. Yang, J. Z. Du, S. Dou, C. Q. Mao, H. Y. Long, J. Wang, *ACS Nano* **2012**, *6*, 771.

[14] X. Z. Yang, S. Dou, T. M. Sun, C. Q. Mao, H. X. Wang, J. Wang, *J. Controlled Release* **2011**, *156*, 203.

[15] a) K. S. Lee, H. C. Chung, S. A. Im, Y. H. Park, C. S. Kim, S. B. Kim, S. Y. Rha, M. Y. Lee, J. Ro, *Breast Cancer Res. Treat.* **2008**, *108*, 241; b) M. E. Davis, Z. Chen, D. M. Shin, *Nat. Rev. Drug Discovery* **2008**, *7*, 771.

[16] a) C. E. Ashley, E. C. Carnes, K. E. Epler, D. P. Padilla, G. K. Phillips, R. E. Castillo, D. C. Wilkinson, B. S. Wilkinson, C. A. Burgard, R. M. Kalinich, J. L. Townson, B. Chackerian, C. L. Willman, D. S. Peabody, W. Wharton, C. J. Brinker, *ACS Nano* **2012**, *6*, 2174; b) F. M. Kievit, O. Veiseh, C. Fang, N. Bhattarai, D. Lee, R. G. Ellenbogen, M. Zhang, *ACS Nano* **2010**, *4*, 4587; c) Y. A. Shieh, S. J. Yang, M. F. Wei, M. J. Shieh, *ACS Nano* **2010**, *4*, 1433; d) A. J. Shuhendler, P. Prasad, M. Leung, A. M. Rauth, R. S. DaCosta, X. Y. Wu, *Adv. Healthcare Mater.* **2012**, *1*, 660.

[17] a) A. N. Lukyanov, T. A. Elbayoumi, A. R. Chakilam, V. P. Torchilin, *J. Controlled Release* **2004**, *100*, 135; b) L. Pourtau, H. Oliveira, J. Thevenot, Y. Wan, A. R. Brisson, O. Sandre, S. Miraux, E. Thiaudiere, S. Lecommandoux, *Adv. Healthcare Mater.* **2013**, *2*, 1420.

[18] X. Chen, X. Wang, Y. Wang, L. Yang, J. Hu, W. Xiao, A. Fu, L. Cai, X. Li, X. Ye, Y. Liu, W. Wu, X. Shao, Y. Mao, Y. Wei, L. Chen, *J. Controlled Release* **2010**, *145*, 17.

[19] S. Nayak, H. Lee, J. Chmielewski, L. A. Lyon, *J. Am. Chem. Soc.* **2004**, *126*, 10258.

[20] V. Bagalkot, L. Zhang, E. Levy-Nissenbaum, S. Jon, P. W. Kantoff, R. Langer, O. C. Farokhzad, *Nano Lett.* **2007**, *7*, 3065.

[21] a) R. E. Bird, K. D. Hardman, J. W. Jacobson, S. Johnson, B. M. Kaufman, S. M. Lee, T. Lee, S. H. Pope, G. S. Riordan, M. Whitlow, *Science* **1988**, *242*, 423; b) J. S. Huston, D. Levinson, M. Mudgett-Hunter, M. S. Tai, J. Novotny, M. N. Margolies, R. J. Ridge, R. E. Bruccoleri, E. Haber, R. Crea, *Proc. Natl. Acad. Sci. U.S.A.* **1988**, *85*, 5879.

[22] X. H. Peng, Y. Wang, D. Huang, Y. Wang, H. J. Shin, Z. Chen, M. B. Spewak, H. Mao, X. Wang, Y. Wang, Z. Chen, S. Nie, D. M. Shin, *ACS Nano* **2011**, *5*, 9480.

[23] Y. D. Yao, T. M. Sun, S. Y. Huang, S. Dou, L. Lin, J. N. Chen, J. B. Ruan, C. Q. Mao, F. Y. Yu, M. S. Zeng, J. Y. Zang, Q. Liu, F. X. Su, P. Zhang, J. Lieberman, J. Wang, E. Song, *Sci. Transl. Med.* **2012**, *4*, 130.

[24] a) C. Qian, Y. Wang, Y. Chen, L. Zeng, Q. Zhang, X. Shuai, K. Huang, *Biomaterials* **2013**, *34*, 6175; b) K. L. Vigor, P. G. Kyrtatos, S. Minogue, K. T. Al-Jamal, H. Kogelberg, B. Tolner, K. Kostarelos, R. H. Begent, Q. A. Pankhurst, M. F. Lythgoe, K. A. Chester, *Biomaterials* **2010**, *31*, 1307.

[25] a) B. Q. Shen, K. Xu, L. Liu, H. Raab, S. Bhakta, M. Kenrick, K. L. Parsons-Reponte, J. Tien, S. F. Yu, E. Mai, D. Li, J. Tibbitts, J. Baudys, O. M. Saadi, S. J. Scales, P. J. McDonald, P. E. Hass, C. Eigenbrot, N. Trung, W. A. Solis, R. N. Fuji, K. M. Flagella, D. Patel, S. D. Spencer, L. A. Khawlil, A. Ebens, W. L. Wong, R. Vandlen, S. Kaur, M. X. Sliwkowski, R. H. Scheller, P. Polakis, J. R. Junutula, *Nat. Biotechnol.* **2012**, *30*, 184; b) J. R. Junutula, H. Raab, S. Clark, S. Bhakta, D. D. Leipold, S. Weir, Y. Chen, M. Simpson, S. P. Tsai, M. S. Dennis, Y. Lu, Y. G. Meng, C. Ng, J. Yang, C. C. Lee, E. Duenas, J. Gorrell, V. Katta, A. Kim, K. McDorman, K. Flagella, R. Venook, S. Ross, S. D. Spencer, W. L. Wong, H. B. Lowman, R. Vandlen, M. X. Sliwkowski, R. H. Scheller, P. Polakis, W. Mallet, *Nat. Biotechnol.* **2008**, *26*, 925.

[26] a) Q. Hu, G. Gu, Z. Liu, M. Jiang, T. Kang, D. Miao, Y. Tu, Z. Pang, Q. Song, L. Yao, H. Xia, H. Chen, X. Jiang, X. Gao, J. Chen, *Biomaterials* **2013**, *34*, 1135; b) A. Beduneau, P. Saulnier, F. Hindre, A. Clavreul, J. C. Leroux, J. P. Benoit, *Biomaterials* **2007**, *28*, 4978.

[27] a) C. Wang, L. Cheng, Z. Liu, *Biomaterials* **2011**, *32*, 1110; b) N. Graf, D. R. Bielenberg, N. Kolishetti, C. Muus, J. Banyard, O. C. Farokhzad, S. J. Lippard, *ACS Nano* **2012**, *6*, 4530; c) P. Zhang, L. Hu, Q. Yin, Z. Zhang, L. Feng, Y. Li, *J. Controlled Release* **2012**, *159*, 429; d) J. Gao, Y. Yu, Y. Zhang, J. Song, H. Chen, W. Li, W. Qian, L. Deng, G. Kou, J. Chen, Y. Guo, *Biomaterials* **2012**, *33*, 270.

[28] Y. Yarden, *Oncology* **2001**, *61*, 1.

[29] D. M. Glover, I. M. Hagan, A. A. Tavares, *Genes Dev.* **1998**, *12*, 3777.

[30] a) B. Spankuch-Schmitt, J. Bereiter-Hahn, M. Kaufmann, K. Strebhardt, *J. Natl. Cancer Inst.* **2002**, *94*, 1863; b) F. Eckerdt, J. P. Yuan, K. Strebhardt, *Oncogene* **2005**, *24*, 267.

[31] Y. Bu, Z. Yang, Q. Li, F. Song, *Oncology* **2008**, *74*, 198.

[32] Z. Poon, D. Chang, X. Y. Zhao, P. T. Hammond, *ACS Nano* **2011**, *5*, 4284.

[33] X. Yang, J. J. Grailer, I. J. Rowland, A. Javadi, S. A. Hurley, D. A. Steeber, S. Gong, *Biomaterials* **2010**, *31*, 9065.

[34] X. G. Li, P. Stuckert, I. Bosch, J. D. Marks, W. A. Marasco, *Cancer Gene Ther.* **2001**, *8*, 555.

[35] P. W. Riddles, R. L. Blakeley, B. Zerner, *Anal. Biochem.* **1979**, *94*, 75.

[36] H. X. Wang, M. H. Xiong, Y. C. Wang, J. Zhu, J. Wang, *J. Controlled Release* **2013**, *166*, 106.

